Potential energy landscape of TIP4P/2005 water

Philip H. Handle, and Francesco Sciortino

Citation: The Journal of Chemical Physics **148**, 134505 (2018); doi: 10.1063/1.5023894
View online: https://doi.org/10.1063/1.5023894
View Table of Contents: http://aip.scitation.org/toc/jcp/148/13
Published by the American Institute of Physics

THE JOURNAL OF CHEMICAL PHYSICS **148**, 134505 (2018)

Potential energy landscape of TIP4P/2005 water

Philip H. Handle and Francesco Sciortino
Department of Physics, Sapienza–University of Rome, Piazzale Aldo Moro 5, I-00185 Roma, Italy

(Received 29 January 2018; accepted 9 March 2018; published online 3 April 2018)

We report a numerical study of the statistical properties of the potential energy landscape of TIP4P/2005, one of the most accurate rigid water models. We show that, in the region where equilibrated configurations can be generated, a Gaussian landscape description is able to properly describe the model properties. We also find that the volume dependence of the landscape properties is consistent with the existence of a locus of density maxima in the phase diagram. The landscape-based equation of state accurately reproduces the TIP4P/2005 pressure-vs-volume curves, providing a sound extrapolation of the free-energy at low T. A positive-pressure liquid-liquid critical point is predicted by the resulting free-energy. *Published by AIP Publishing.* https://doi.org/10.1063/1.5023894

I. INTRODUCTION

The potential energy landscape (PEL) framework offers an intuitive description of the physics of low temperature (T) liquids.[1] It is based on the idea that molecular motions at low T can be split into anharmonic vibrations around potential energy local minima (the so-called inherent structures,[2] ISs) and infrequent visits of several different such minima.[3]

Computer simulations have been crucial in supporting the PEL approach.[2] Efficient conjugate gradient minimization algorithms provide the possibility to associate with each equilibrium configuration its IS and to study the connection between the system dynamics and the PEL.[4,5] The onset of a two-step relaxation decay of correlation functions has been shown to coincide with the onset of the PEL dominated region,[6] i.e., with the temperature below which the energy $e_{\rm IS}$ of the sampled IS becomes T dependent. As envisioned by Goldstein,[3] below this T, deeper and deeper PEL basins are visited on supercooling.

The power of the PEL approach is rooted not only in the possibility of closely comparing the theoretical assumptions with numerical results, but more importantly in the possibility of developing a formal description of the thermodynamics of supercooled liquids. The number of basins of depth $e_{\rm IS}$ and their shape are key ingredients to express the liquid partition function (and hence the free energy) in terms of statistical properties of the PEL.[7–12] Modeling of such quantities (supported by a one-to-one comparison with numerical results) offers the possibility to predict, with clear assumptions, the thermodynamics of supercooled liquids[8] and in limited cases even the thermodynamics in out-of-equilibrium conditions.[13] In addition, the analysis of the ISs provides insights into the glass phases of the material studied.

An interesting application of the PEL framework is offered by the study of water, a liquid which continues to challenge contemporary science due to its complex behavior.[14–17] A hallmark of this complexity is the well-known maximum in density at ambient pressure (P) around 4 °C and the minima displayed by the isobaric heat capacity and the isothermal compressibility. In addition, these response functions show a marked change in supercooled states. For state-of-the-art results, see, for example, Refs. 18 and 19. Several recent reviews[15–17,20] discuss in detail the principal thermodynamic scenarios compatible with the experimental observation: (i) the Speedy limit of stability scenario[21] (recently observed in numerical studies of colloidal model particles[22,23]), (ii) the singularity free scenario,[24] and (iii) the liquid-liquid critical point (LLCP) scenario.[25] This last scenario, depending on the locus of the second critical point, changes into the critical point free scenario when the critical pressure approaches the spinodal pressure.[26]

The statistical properties of the PEL responsible for the density maxima and all other related[19,24,27,28] anomalies have been previously discussed.[29] As reviewed in Sec. II, within the harmonic Gaussian PEL hypothesis, the volume dependence of just one of the landscape parameters suffices to discriminate liquids with and without density anomalies. An investigation of the PEL of the SPC/E model[30] was shown to be consistent with theoretical predictions, suggesting the presence of a low T liquid-liquid critical point.[29] In more recent years, significantly improved classic rigid-water models have been proposed, which are able to better reproduce water's physical properties.[31] Among this class of model potentials, TIP4P/2005[32] has emerged as the present-day optimal choice. We present here the first detailed PEL investigation of the TIP4P/2005 model with the aims of (i) confirming the quality of the Gaussian PEL assumption in modeling the statistical properties of the landscape; (ii) incorporating the anharmonic contribution to the basin shape into the equation of state (EOS) which was previously neglected; (iii) confirming the connection between statistical properties of the landscape and density anomalies; (iv) providing a sound PEL supported extrapolation of the model EOS to investigate the possibility of a liquid-liquid critical point in TIP4P/2005.[33–40] In addition, the evaluation of the IS provides information on the structural properties of amorphous water.[15,41–45]

II. THE GAUSSIAN PEL APPROACH

We base our study on the PEL framework, introduced by Stillinger and Weber.[2,46] Within this framework, the multidimensional potential energy surface $U(\vec{r}^N, \phi^N, \theta^N, \psi^N)$, a function of the center of mass positions $\vec{r}$ and orientations (given by the Euler angles ϕ, θ, ψ) of all N molecules, is split into *basins*. A basin is defined as the set of all configurations which under a steepest descent path end up in the same local potential energy minimum. Such minimum configuration is named *inherent structure* (IS) and its associated energy e_{IS}. Thus, $U(\vec{r}^N, \phi^N, \theta^N, \psi^N)$ can be written as

$$U(\vec{r}^N, \phi^N, \theta^N, \psi^N) = e_{\mathrm{IS}} + \Delta U(\vec{r}^N, \phi^N, \theta^N, \psi^N), \tag{1}$$

where $\Delta U(\vec{r}^N, \phi^N, \theta^N, \psi^N)$ quantifies the energy associated with the thermal vibration around the IS. Grouping all basins with the same e_{IS}, the canonical partition function of the system can be written as[46,47]

$$Z(T,V) = \int_{e_{\mathrm{IS}}} \Omega(e_{\mathrm{IS}})\mathrm{d}e_{\mathrm{IS}}\, \mathrm{e}^{-\beta F_{\mathrm{basin}}(e_{\mathrm{IS}},T,V)}, \tag{2}$$

where $\Omega(e_{\mathrm{IS}})\mathrm{d}e_{\mathrm{IS}}$ is the number of basins with IS energy between e_{IS} and $e_{\mathrm{IS}} + \mathrm{d}e_{\mathrm{IS}}$, $F_{\mathrm{basin}}(e_{\mathrm{IS}}, T, V)$ is the average free energy of a basin of depth e_{IS}, and β is $1/k_{\mathrm{B}}T$ with k_{B} being Boltzmann's constant. All basins containing a significant amount of crystalline order are by definition not included in the integration over phase space in Eq. (2).

A formal expression for the basin free energy can be written as

$$F_{\mathrm{basin}}(e_{\mathrm{IS}},T,V) = e_{\mathrm{IS}} + F_{\mathrm{harm}}(e_{\mathrm{IS}},T,V) + F_{\mathrm{anh}}(e_{\mathrm{IS}},T,V), \tag{3}$$

where the first term on the rhs is the basin minimum energy, the second term accounts for the harmonic vibrations around the minimum (and their e_{IS} dependence), while the last term accounts for the remaining anharmonic contribution to the basin free energy. The harmonic free energy can be calculated as

$$\beta F_{\mathrm{harm}}(e_{\mathrm{IS}},T,V) \equiv \left\langle \sum_{i=1}^{6N-3} \ln\left(\beta\hbar\omega_i(e_{\mathrm{IS}})\right) \right\rangle_{e_{\mathrm{IS}}}, \tag{4}$$

where $\omega_i(e_{\mathrm{IS}})$ are the normal mode frequencies and $\hbar$ is Planck's constant. To separate the T and the e_{IS} dependence, we write

$$\beta F_{\mathrm{harm}}(e_{\mathrm{IS}},T,V) = (6N-3)\ln(\beta A_0) + \mathcal{S}(e_{\mathrm{IS}},V), \tag{5}$$

where

$$\mathcal{S}(e_{\mathrm{IS}},V) = \left\langle \sum_{i=1}^{6N-3} \ln\left(\frac{\hbar\omega_i(e_{\mathrm{IS}},V)}{A_0}\right) \right\rangle_{e_{\mathrm{IS}}}. \tag{6}$$

The latter is called the basin shape function, and $A_0 \equiv 1$ kJ mol^{-1} ensures that the arguments of the logarithms bare no units.

The expressions derived so far are formally exact. To proceed further, one needs to model the statistical properties of the landscape[8,9,12,48] as well as a description of the harmonic and anharmonic contributions. This is performed by comparing step by step the theoretical assumption with numerical results.

In the following, we review the EOS for a Gaussian landscape with minimal assumptions on the harmonic and anharmonic contributions and show that the resulting EOS properly models the TIP4P/2005 pressure-volume relation. In a Gaussian landscape, for each V, three parameters describe the PEL statistical properties: the total number of basins $\mathrm{e}^{\alpha N}$ (where N is the number of molecules), the most probable IS energy E_0, and the variance σ^2, resulting in

$$\Omega(e_{\mathrm{IS}})\mathrm{d}e_{\mathrm{IS}} = \frac{\mathrm{e}^{\alpha N}}{\sqrt{2\pi\sigma^2}} \mathrm{e}^{-\frac{(e_{\mathrm{IS}}-E_0)^2}{2\sigma^2}} \mathrm{d}e_{\mathrm{IS}}. \tag{7}$$

We further assume that (i) the shape function is linear with e_{IS} (as previously found in several investigated models[29,49,50]),

$$\mathcal{S}(e_{\mathrm{IS}},V) = a(V) + b(V)e_{\mathrm{IS}}, \tag{8}$$

where a and b represent the (V-dependent) coefficients of the linear expansion; (ii) the anharmonic free energy is independent of e_{IS}. Thus, we can write the anharmonic potential energy as a polynomial in T starting from a quadratic term

$$U_{\mathrm{anh}}(T,V) = \sum_{i=2}^{i_{\mathrm{max}}} c_i(V)T^i, \tag{9}$$

where c_i represent the respective (V-dependent) coefficients. Solving $\mathrm{d}S_{\mathrm{anh}}/\mathrm{d}U_{\mathrm{anh}} = 1/T$, the anharmonic entropy is written as

$$S_{\mathrm{anh}}(T,V) = \sum_{i=2}^{i_{\mathrm{max}}} \frac{i}{i-1} c_i T^{i-1}. \tag{10}$$

Thus the anharmonic free energy is

$$\begin{aligned} F_{\mathrm{anh}}(T,V) &= U_{\mathrm{anh}}(T,V) - TS_{\mathrm{anh}}(T,V) \\ &= \sum_{i=2}^{i_{\mathrm{max}}} c_i T^i \left(1 - \frac{i}{i-1}\right). \end{aligned} \tag{11}$$

Other approximations, which do not require the assumption of e_{IS} independence of the anharmonic free energy, have been proposed in the past,[51] but they do require a larger number of parameters.

Within the outlined approximation, the T dependence of the average IS energy E_{IS} at a given V can be formally written as

$$E_{\mathrm{IS}}(T) = E_0 - b\sigma^2 - \frac{\sigma^2}{k_{\mathrm{B}}T}, \tag{12}$$

where E_0, σ^2, and b depend all on V. Thus, in a Gaussian landscape, E_{IS} is linear in $1/T$, a prediction which can be tested numerically.

The configurational entropy can also be expressed in terms of V-dependent PEL quantities as

$$\frac{S_{\mathrm{conf}}(T)}{k_{\mathrm{B}}} \equiv \ln\Omega(E_{\mathrm{IS}}(T)) = \alpha N - \frac{\sigma^2(b+\beta)^2}{2} \tag{13}$$

which again provides a stringent numerical test of the T-dependence of S_{conf}.

Defining the Kauzmann temperature T_{K} as the temperature at which $S_{\mathrm{conf}} = 0$, one finds

$$k_{\mathrm{B}} T_{\mathrm{K}} = \left(\sqrt{\frac{2\alpha N}{\sigma^2}} - b \right)^{-1}. \tag{14}$$

Below T_K, the system is trapped in the basin of depth

$$e_{\mathrm{K}} \equiv E_{\mathrm{IS}}(T_{\mathrm{K}}) = E_0 - \sqrt{2\alpha N}\sigma. \tag{15}$$

Finally we note that the validity of the Gaussian landscape at temperatures significantly lower than the one we have investigated is not guaranteed. Assuming quantized excitations around the lowest disordered energy state, the low T landscape would be better described by a logarithmic landscape.[11]

III. THE PEL EQUATION OF STATE

A benefit in using the Gaussian landscape approach lies in the possibility to analytically derive an EOS. This EOS can be expressed in terms of volume derivatives of the PEL parameters.[8,47,52] Past studies, however, used only the harmonic Gaussian parameters to formulate the EOS. We here derive an expression including terms arising from anharmonic corrections. The PEL free energy can be written as

$$F = E_{\mathrm{IS}} - TS_{\mathrm{conf}} + F_{\mathrm{harm}} + F_{\mathrm{anh}}. \tag{16}$$

The first two terms can be condensed in a free energy of the inherent structure F_{IS}.

Hence the pressure can be expressed as

$$P = -\frac{\partial F}{\partial V} = -\frac{\partial F_{\mathrm{IS}}}{\partial V} - \frac{\partial F_{\mathrm{harm}}}{\partial V} - \frac{\partial F_{\mathrm{anh}}}{\partial V}. \tag{17}$$

We now look at each term separately. The volume derivative of F_{IS} is

$$\begin{aligned} -\frac{\partial F_{\mathrm{IS}}}{\partial V} &= -\frac{\partial}{\partial V}\left(E_{\mathrm{IS}} - TS_{\mathrm{conf}}\right) \\ &= -\frac{\partial (E_0 - b\sigma^2)}{\partial V} + \frac{1}{k_{\mathrm{B}}T}\frac{\partial \sigma^2}{\partial V} + T\frac{\partial S_{\mathrm{conf}}}{\partial V}. \end{aligned} \tag{18}$$

Using Eq. (13), we further find

$$\begin{aligned} T\frac{\partial S_{\mathrm{conf}}}{\partial V} &= k_{\mathrm{B}}T\frac{\partial}{\partial V}\left(\alpha N - \frac{\sigma^2 (b+\beta)^2}{2}\right) \\ &= k_{\mathrm{B}}T\frac{\partial}{\partial V}\left(\alpha N - \frac{b^2\sigma^2}{2}\right) - \frac{\partial (b\sigma^2)}{\partial V} - \frac{1}{2k_{\mathrm{B}}T}\frac{\partial \sigma^2}{\partial V}. \end{aligned} \tag{19}$$

Finally, bringing Eqs. (18) and (19) together and grouping the terms according to their respective temperature dependence,

$$-\frac{\partial F_{\mathrm{IS}}}{\partial V} = -\frac{\partial E_0}{\partial V} + Tk_{\mathrm{B}}\frac{\partial}{\partial V}\left(\alpha N - \frac{b^2\sigma^2}{2}\right) + \frac{1}{T}\frac{1}{2k_{\mathrm{B}}}\frac{\partial \sigma^2}{\partial V}. \tag{20}$$

Next we perform the same procedure for F_{harm} using Eqs. (8) and (12),

$$\begin{aligned} -\frac{\partial F_{\mathrm{harm}}}{\partial V} &= -k_{\mathrm{B}}T\frac{\partial \mathcal{S}}{\partial V} \\ &= -k_{\mathrm{B}}T\frac{\partial}{\partial V}\left(a + bE_0 - b^2\sigma^2 - \frac{b\sigma^2}{k_{\mathrm{B}}T}\right). \end{aligned} \tag{21}$$

Sorting the terms according to their respective temperature dependence, we find

$$-\frac{\partial F_{\mathrm{harm}}}{\partial V} = \frac{\partial}{\partial V}b\sigma^2 - Tk_{\mathrm{B}}\frac{\partial}{\partial V}(a + bE_0 - b^2\sigma^2). \tag{22}$$

The anharmonic contribution to the pressure arises from the volume derivative of the c_i coefficient in Eq. (11),

$$-\frac{\partial F_{\mathrm{anh}}}{\partial V} = \sum_{i=2}^{i_{\max}} T^i \frac{\partial c_i(V)}{\partial V}\left(\frac{i}{i-1} - 1\right). \tag{23}$$

Since all contributions could be separated into terms of different temperature dependence, the equation of state including anharmonic corrections reads

$$P(T,V) = \sum_{i=-1}^{i_{\max}} \mathcal{P}_{T^i}(V) T^i, \tag{24}$$

where we have defined

$$\mathcal{P}_{T^{-1}}(V) = \frac{1}{2k_{\mathrm{B}}}\frac{\mathrm{d}}{\mathrm{d}V}\sigma^2, \tag{25}$$

$$\mathcal{P}_{T^{0}}(V) = -\frac{\mathrm{d}}{\mathrm{d}V}\left(E_0 - b\sigma^2\right), \tag{26}$$

$$\mathcal{P}_{T^{1}}(V) = k_{\mathrm{B}}\frac{\mathrm{d}}{\mathrm{d}V}\left(\alpha N - a - bE_0 + \frac{b^2\sigma^2}{2}\right), \tag{27}$$

$$\mathcal{P}_{T^{i\geq 2}}(V) = \left(\frac{i}{i-1} - 1\right)\frac{\mathrm{d}}{\mathrm{d}V}c_i(V). \tag{28}$$

For reasons that will be clear next, we notice that $\mathcal{P}_{T^{-1}}(V)$ involves only the V derivative of σ^2.

From the mathematical structure of Eq. (24), it is clear that, if the system moves along an isochore, the high T behavior is controlled by the $i_{\max}$ order term in T. The behavior at low T however is controlled by the $\mathcal{P}_{T^{-1}}T^{-1}$ term. One can also see that the pressure along an isochore must display a minimum if $\mathcal{P}_{T^{-1}} > 0$. In this case, a density maximum exists. Indeed, according to a Maxwell relation, $\partial P/\partial T|_V = 0$ corresponds to $\partial V/\partial T|_P = 0$, i.e., to a density extremum. Hence, the condition for the existence of density maxima ($\mathcal{P}_{T^{-1}} > 0$) in the PEL formalism corresponds to $\mathrm{d}\sigma^2/\mathrm{d}V > 0$ [see Eq. (25)]. Thus, in the Gaussian landscape, liquids with density anomalies must be characterized by a V-range where σ^2 increases with V.

IV. SIMULATION DETAILS

A. NVT simulations

We perform NVT simulations of 1000 TIP4P/2005 molecules in a cubic box utilising GROMACS 5.1.2[53] with a leap-frog integrator using a time step of 1 fs. The temperature is controlled using a Nosé-Hoover thermostat[54,55] with a time constant of 0.2 ps. For the Coulombic interactions, we use a particle mesh Ewald treatment[56] with a Fourier spacing of 0.1 nm. For both the Lennard-Jones (LJ) and the real space Coulomb interactions, a cutoff of 0.85 nm is used. Lennard-Jones interactions beyond 0.85 nm have been included assuming a uniform fluid density. Finally, we maintain the bond constraints using the LINCS (Linear Constraint Solver) algorithm[57] of 6th order with one iteration to correct for rotational lengthening. We investigate 14 different densities from 0.9 to 1.42 g/cm^3 and seven different Ts between 200 and 270 K. We performed equilibration runs up to 100 ns followed by equally long production runs. Equally spaced configurations from the production runs have been used in the following analysis.

B. Inherent structures

To generate the IS configuration, we minimise the potential energy of the system with a conjugate gradient method (evolving the centre of mass and the orientation of the particles around their principal axes). At least 30 configurations extracted from each trajectory were minimised. We also evaluate the normal modes of all the found inherent structures via the numerical determination of the Hessian, the $6N \times 6N$ matrix of the second derivatives of the potential energy as a function of the molecule centre of mass and principal axes. Both conjugate gradient minimization and Hessian evaluation have been performed with our own code.

C. Free energy

We evaluate the harmonic free energy (F_{harm}) of all different IS according to Eq. (4), starting form the density of states calculated by diagonalising the Hessian matrix. The free energy of TIP4P/2005 in the liquid state (F_{liq}) is evaluated by performing thermodynamic and Hamiltonian integration,[59] starting from the known reference free energy of an ideal gas of water-shaped molecules $F_{\mathrm{id}}(T, V, N)$. Specifically,

$$\beta F_{\mathrm{id}}(T,V,N) = -\ln Z_{\mathrm{id}}(T,V,N), \tag{29}$$

where the partition function

$$Z_{\mathrm{id}}(T,V,N) = \frac{Z_{\mathrm{T}} Z_{\mathrm{R}}}{N!} \tag{30}$$

can be split in a translational part

$$Z_{\mathrm{T}} = \left(V \left(\frac{2\pi m k_{\mathrm{B}} T}{h^2} \right)^{\frac{3}{2}} \right)^N \tag{31}$$

and a rotational part

$$Z_{\mathrm{R}} = \left(\frac{1}{2} \left(\frac{8\pi^2 k_{\mathrm{B}} T}{h^2} \right)^{\frac{3}{2}} \left(\pi I_x I_y I_z \right)^{\frac{1}{2}} \right)^N, \tag{32}$$

where m is the mass of the water molecule and I_x, I_y, and I_z are the moments of inertia along the three principal axes. The factor $\frac{1}{2}$ in front of Z_{R} accounts for the water molecule's C_{2v} symmetry.[60] For future reference, we note that the molecular ideal gas (non-interacting) free energy at $T_{\mathrm{ref}} = 3000$ K and $\rho_{\mathrm{ref}} = 1.1$ g/cm^3 is −481.15 kJ/mol.

To evaluate the free energy of a system of water molecules (e.g., with centre of mass and orientational degrees of freedom) interacting only via a Lennard-Jones interaction $U_{\mathrm{LJ}}(r)$ between the oxygen sites (we use the $\sigma = 0.315\,89$ nm and the $\epsilon = 774.9$ J mol^{-1} of the TIP4P/2005 model[32]) we perform a thermodynamic integration along a path of constant density ρ_{ref} from infinite T down to T_{ref} of the isotropic pair potential $U(r)$ defined as[61]

$$U(r) = \min(U_{\mathrm{LJ}}(r), U_{\mathrm{cutoff}}). \tag{33}$$

This potential coincides with the $U_{\mathrm{LJ}}(r)$ potential for all intermolecular distances for which $U_{\mathrm{LJ}}(r) < U_{\mathrm{cutoff}}$, and it is constant and equal to U_{cutoff} otherwise. With this choice, the divergence of the potential energy for configurations in which some intermolecular separations vanish (which would otherwise be probed at very high T) is eliminated and the infinite T limit is properly approximated by an ideal gas of molecules at the same density. Specifically, we choose $U_{\mathrm{cutoff}} = 100RT_{\mathrm{ref}}$ J/mol (R being the ideal gas constant), corresponding to a interparticle distance of $r_{\mathrm{cutoff}} = 0.180\,33$ nm.

The fluid free energy (per particle) is calculated as

$$F_{\mathrm{LJ}}(T,V,N) = F_{\mathrm{id}}(T,V,N) + k_{\mathrm{B}} T_{\mathrm{ref}} \int_0^{\beta_{\mathrm{ref}}} \langle U \rangle_\beta \mathrm{d}\beta, \tag{34}$$

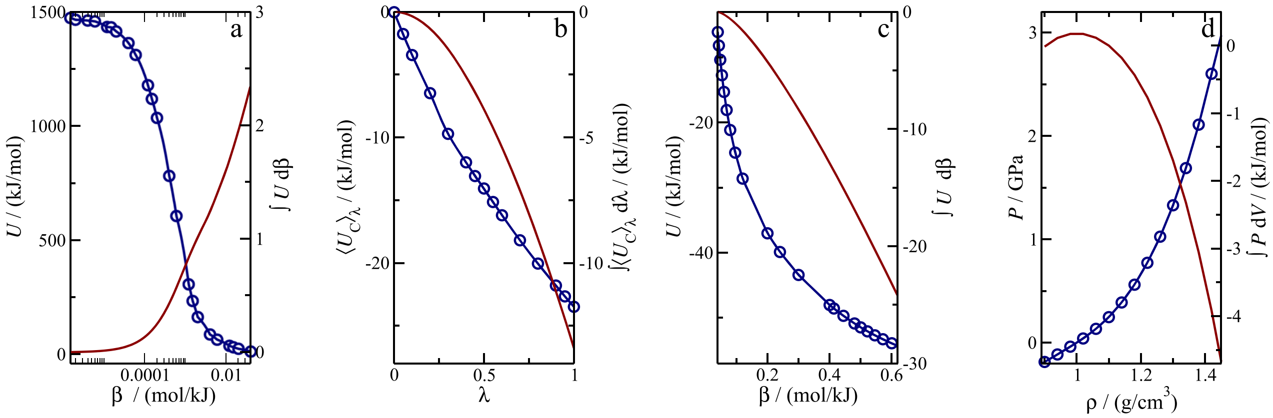

FIG. 1. Steps in the thermodynamic integration process requested for the evaluation of the TIP4P/2005 free energy. Panel (a) shows the thermodynamic integration from infinite T (ideal gas) to $T_{\mathrm{ref}} = 3000$ K of a system of particles at $\rho_{\mathrm{ref}} = 1.1$ g/cm^3, interacting according to the potential energy in Eq. (33). Panel (b) shows the Hamiltonian λ integration from LJ to TIP4P/2005 [see Eq. (35)]. Panel (c) shows the thermodynamic integration from T_{ref} down to the studied T at ρ_{ref}. Panel (d) shows the thermodynamic integration from ρ_{ref} to the studied ρ at $T = 270$ K. In all panels, the blue line represents the integrand and the red line represents the running integral.

where the integration goes from infinite T to $\beta_{\rm ref} = 1/k_B T_{\rm ref}$. Figure 1(a) shows the resulting β dependence of $\langle U\rangle_\beta$ evaluated on a mesh of 23 points and the corresponding running integral $\int_0^\beta \langle U\rangle_\beta \mathrm{d}\beta$. The free energy of water-shaped molecules interacting only via a Lennard-Jones interaction at $T_{\rm ref}$ and $\rho_{\rm ref}$ is −422.84 kJ/mol.

Next we evaluate the free energy change from the LJ to the TIP4P/2005 model at $\rho_{\rm ref}$ and $T_{\rm ref}$ via Hamiltonian integration interpolating from LJ to TIP4P/2005. Hence we perform simulations based on the potential energy $U_{\rm LJ} + \lambda(U_{\rm TIP4P/2005} - U_{\rm LJ})$ for 15 different λ values. In this way, the electrostatic interactions are progressively turned on. We note that the separation of the thermodynamic integration in two parts (from ideal gas to LJ and from LJ to TIP4P/2005), while not explicitly necessary, has been implemented to better control the convergence of the two contributions.[62]

The resulting TIP4P/2005 free energy ($F_{\rm liq}$) can be calculated as

$$F_{\rm liq}(T, V, N) = F_{\rm LJ}(T, V, N) + \int_0^1 \langle U_C\rangle_\lambda \,\mathrm{d}\lambda, \qquad (35)$$

where $\langle U_C\rangle_\lambda$ is the canonical average of the potential energy difference $U_{\rm TIP4P/2005} - U_{\rm LJ}$ evaluated in a simulation with potential energy $U_{\rm LJ} + \lambda(U_{\rm TIP4P/2005} - U_{\rm LJ})$. Figure 1(b) shows $\langle U_C\rangle_\lambda$ and the corresponding integral. As a result of the integration, we estimate $F_{\rm liq}(\rho_{\rm ref}, T_{\rm ref}) = -436.23$ kJ mol^{-1}. From this reference point, we then calculate via standard thermodynamic integration along isochores [see Fig. 1(c) for $\rho_{\rm ref}$] and/or along isotherms [see Fig. 1(d) for $T = 270$ K] the TIP4P/2005 free energy at any T and ρ. As a reference for future studies, we report the resulting free-energy in the range 200-270 K for all investigated densities in Appendix A.

From the free energy $F_{\rm liq}$ and the total energy of the liquid $E_{\rm liq}$, the entropy can be calculated from

$$S_{\rm liq} = \frac{E_{\rm liq} - F_{\rm liq}}{T}. \qquad (36)$$

V. RESULTS

A. Minima of the TIP4P/2005

In this section, we provide information on the structure of the IS, describing the IS energies, the static structure factor between the oxygen centres $S(q)$, and the local curvature of the potential energy around the IS [i.e., the vibrational density of states (VDOSs)]. Since the ISs are essentially realisations of the possible glasses of a material, the following structural data provide information on the possible structure and vibrational dynamics of water glasses.

Figure 2 shows the calculated IS energies for all studied state points. As expected, deeper and deeper basins are explored on cooling. The deepest ISs are sampled at the lowest explored density ($\rho \approx 0.9$ g/cm^3), revealing the optimal density for the build up of the hydrogen-bonded network. Interestingly, a region of negative curvature of $E_{\rm IS}$ vs. ρ is present at low T, a first indication of an energetic destabilisation of the liquid.[63,64]

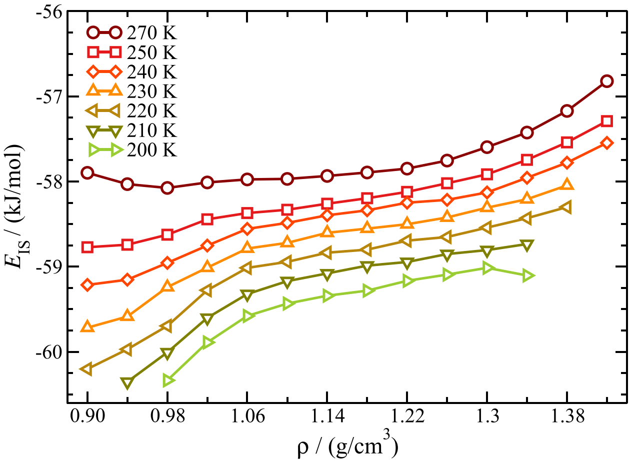

FIG. 2. Average inherent structure energy $E_{\rm IS}$ for all studies state points.

Figure 3 shows $S(q)$ for different densities at $T = 220$ K. Being evaluated in the local minimum, the IS $S(q)$ reflects the static correlation present in the IS, in the absence of any thermal broadening. A clear progression of the structure on increasing density is observed. The signature of the tetrahedral ordering, which show in the $S(q)$ as a pre-peak around 17 nm^{-1} and a main peak around 31 nm^{-1}, progressively disappears in favour of a main peak around 25 nm^{-1} at densities so high that the hydrogen bond network is strongly perturbed. The inset shows the low q region, to provide a quantification of the IS compressibility [related to $S(0)$]. A clear maximum in the density dependence of $S(q)$ at the smallest accessible q value appears, signalling the presence of an extremum in the structural component of the isothermal compressibility. The density fluctuations implicit in the structure achieve their maximum value when $\rho \approx 1.02$ g/cm^3. We also note (see the inset of Fig. 3) that the extrapolation of $S(q)$ at vanishing wavevectors reaches values of the order of 10^{-2} for both the network density ($\rho = 0.9$) and the highest studied density ($\rho = 1.42$ g/cm^3). The vanishing of $S(0)$ in disordered systems has been interpreted as evidence of hyper-uniformity.[65]

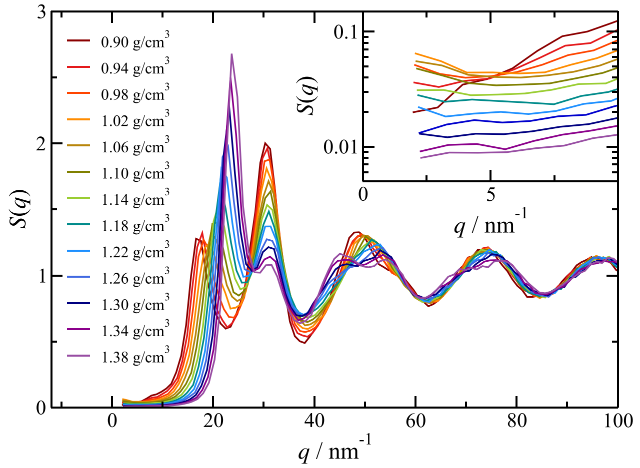

FIG. 3. Oxygen-oxygen structure factor evaluated in the IS at all studied densities at $T = 220$ K. The inset enlarges the low q limit.

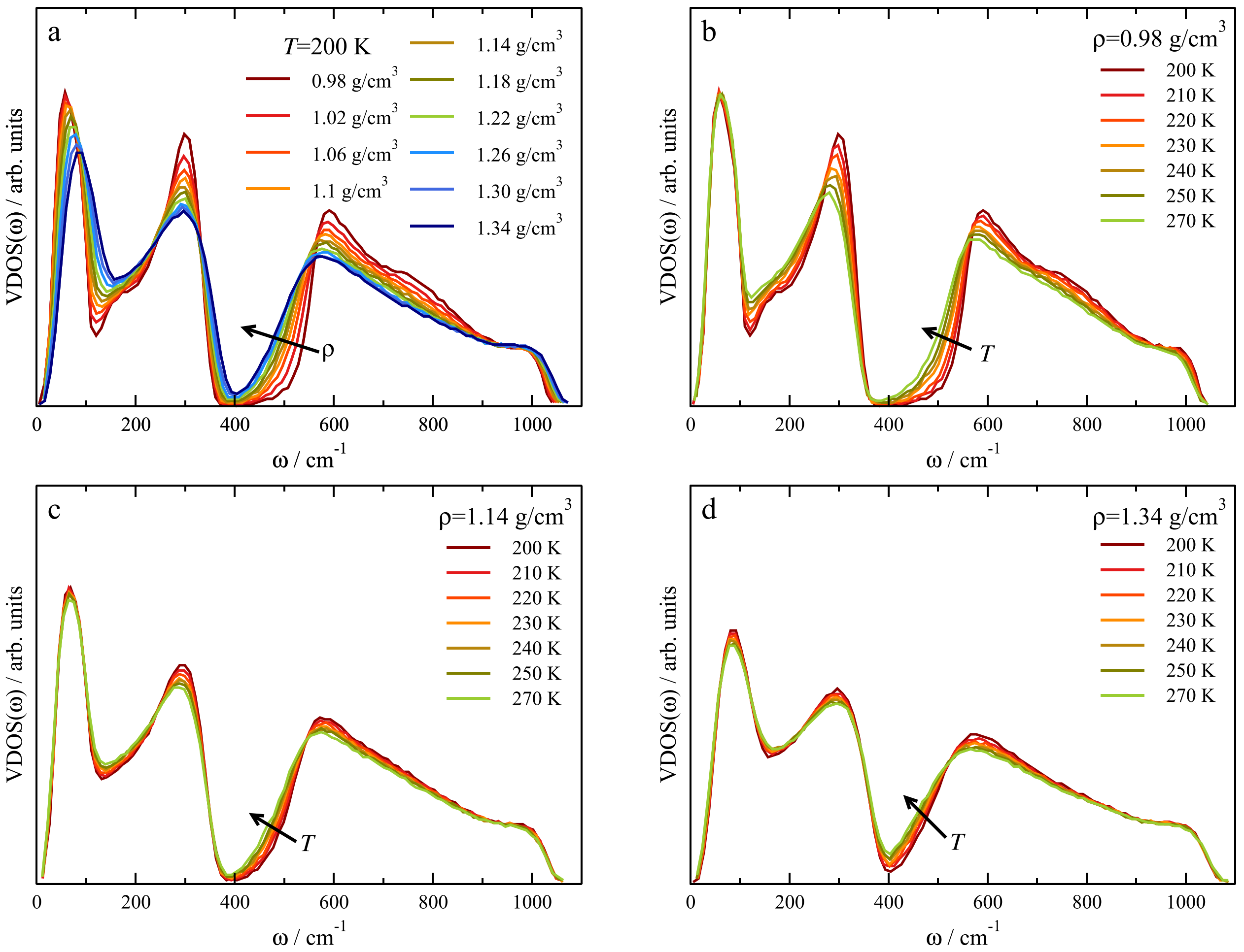

FIG. 4. Vibrational density of states resulting from the diagonalization of the Hessian matrix. Panel (a) shows the density dependence at $T = 200$ K. Panels (b)–(d) report the T dependence at $\rho = 0.98$, $\rho = 1.14$, and $\rho = 1.34$ g/cm^3, respectively.

Recently, it has also been suggested that the structure factor of amorphous ices shows strong signatures of hyperuniformity.[66]

Figure 4 shows the vibrational density of states (VDOS), in harmonic approximation, for several ρ and T, resulting from diagonalising the Hessian matrix in the IS. Previous evaluation of the TIP4P/2005 VDOS in a limited frequency range had been based on Fourier transform of the oxygen velocity autocorrelation functions.[67] The VDOS enters in the evaluation of the basin harmonic vibrational entropy. In all cases, a clear separation between the low-frequency translational bonds ($\omega < 400$ cm^{-1}) and the higher frequency librational bands ($\omega > 400$ cm^{-1}) is observed. Figure 4 shows that the T dependence of the VDOS is more significant at $\rho = 0.98$ g/cm^3, where the development of the tetrahedral networks takes place on cooling and less significant at $\rho = 1.34$ g/cm^3, where the structure of the system is less dependent on the hydrogen bond formation, as clearly indicated by $S(q)$. The data in Fig. 4(a) show that instead a strong density dependence is observed at low T. The low frequency part of the VDOS behaves as ω^2 as expected in the Debye limit.

To evaluate the e_{IS} dependence of the basin shape in harmonic approximation, we evaluate the function $\mathcal{S}$ [cf. Eq. (6)]. For all densities, $\mathcal{S}$ is linear in e_{IS} (Fig. 5), providing a simple quantification of the basin dependence of the free energy [Eq. (8)] via the intercept a and slope b. The basin shape for TIP4P/2005 is similar to the results for SPC/E[49]

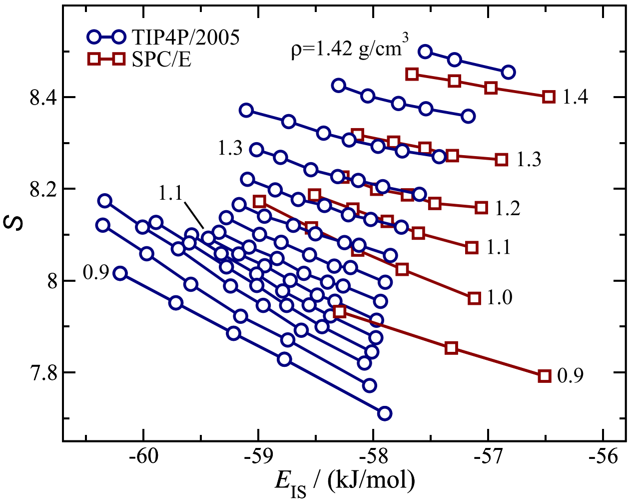

FIG. 5. E_{IS} dependence of the shape function $\mathcal{S}$ (per particle) for all studied densities in comparison with results for SPC/E from Ref. 49.

reproduced also in Fig. 5. The TIP4P/2005 shape is only shifted down in $\mathcal{S}$ and e_{IS}. This similarity is also reflected in the fitting parameters a and b for both models as will be shown below.

B. Evaluating the PEL parameters

Figure 6 shows E_{IS} as a function of $1/T$ for TIP4P/2005. This figure, and the following, also show corresponding results for the SPC/E model of water, the only other water model for which a detailed PEL study has been previously performed.[58] At all densities, E_{IS} is well described by a linear $1/T$ dependence, consistent with the predictions of Eq. (12). This supports the assumption of a Gaussian landscape description of the statistical properties of the PEL and provides a straightforward measure of the important landscape parameter σ^2. The TIP4P/2005 data are consistently smaller than the SPC/E data, but the overall trend of the two models is very similar (e.g., the curve at $\rho = 0.9$ g/cm^3 is the steepest in both cases).

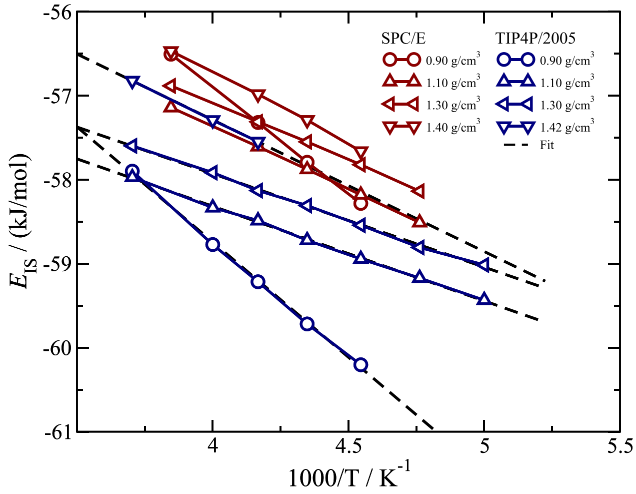

FIG. 6. Inverse temperature dependence of E_{IS} for selected densities in comparison with results for SPC/E from Ref. 58 at similar densities.

From the value of the parameters obtained performing linear representation of the data reported in Figs. 5 and 6, the density (or volume) dependence of the Gaussian PEL parameters σ^2 [Eq. (12)] and E_0 [Eq. (12)] can be evaluated. The results are shown in Fig. 7. E_0 shows the expected minimum, indicating an optimal density ($\rho \approx 1.1$ g/cm^3) for energetic stabilisation, resulting from the compensation between the repulsive contributions (relevant at high densities) and weakening of the attraction on stretching for low densities. More interesting is the minimum observed in the ρ (or V) dependence of σ^2 which, as previously discussed, provides the landscape

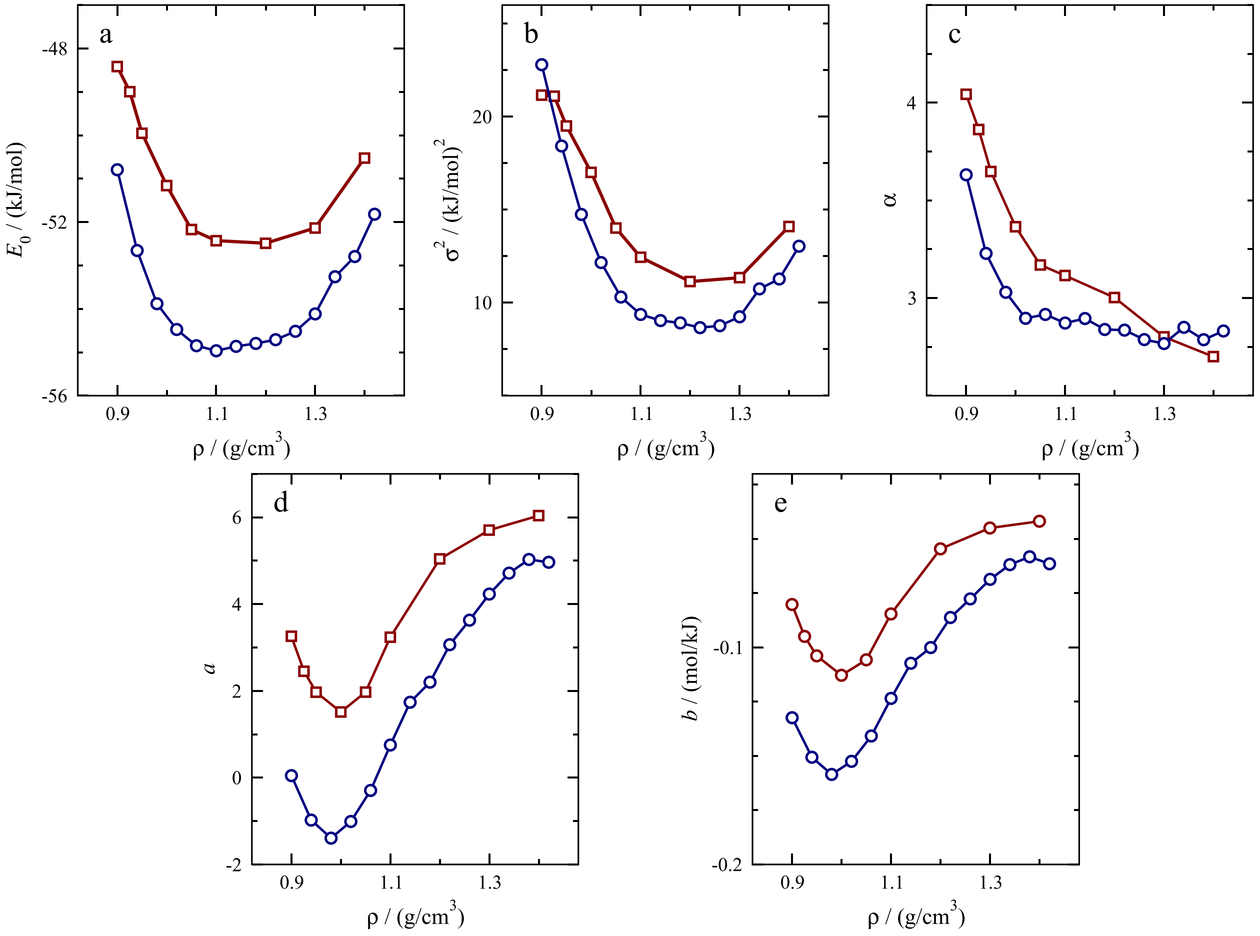

FIG. 7. Density dependence of the landscape parameters E_0, σ^2, α, a, and b in comparison with corresponding data for SPC/E from Ref. 29.

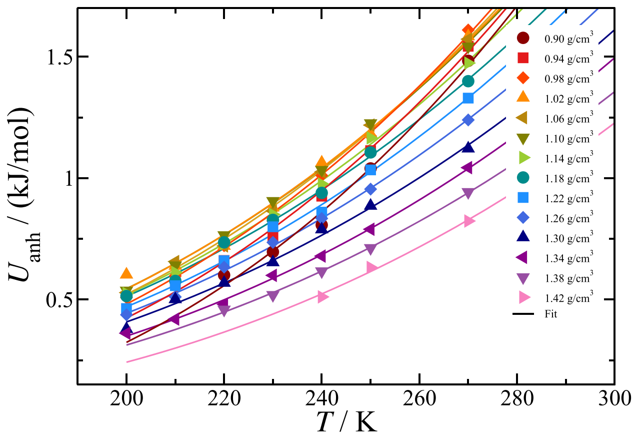

FIG. 8. Temperature dependence of the anharmonic potential energy for several different densities and the associated polynomial fit $c_2(V)T^2 + c_3(V)T^3$, see Eq. (9).

signature of anomalous behavior. The data shown in Fig. 7(b) show that density anomalies are expected in the range $0.9 < \rho < 1.2$ g/cm^3, where $d\sigma^2/dV$ is positive. Figures 7(d) and 7(e) show, respectively, the ρ dependence of the linear fit of $\mathcal{S}$.

To calculate α, we exploit Eq. (13) and evaluate α as the difference between $S_{\rm conf}$ and a quantity dependent only on the previously calculated b and σ^2. $S_{\rm conf}$ is the difference between the entropy of the liquid $S_{\rm liq}$ and the vibrational entropy of the explored basins $S_{\rm harm} + S_{\rm anh}$ (harmonic and anharmonic vibrations around the inherent structures) and can be thus written as

$$S_{\rm conf} = S_{\rm liq} - S_{\rm harm} - S_{\rm anh}. \qquad (37)$$

All three contributions on the rhs are available: $S_{\rm liq}$ from Eq. (36), $S_{\rm harm}$ can be evaluated subtracting from $F_{\rm harm}$ [Eq. (4)] the harmonic potential energy $(6N-3)k_BT$, and $S_{\rm anh}$ according to Eq. (10). The evaluation of $S_{\rm anh}$ requires the preliminary modeling of the T dependence of the anharmonic potential energy $U_{\rm anh} \equiv U_{\rm TIP4P/2005} - E_{\rm IS} - (6N-3)k_BT/2$. Figure 8 shows that $U_{\rm anh}$ vs. T is well represented by Eq. (9) with $i_{\rm max} = 3$ (i.e., $U_{\rm anh} = c_2(V)T^2 + c_3(V)T^3$).

Figure 9 shows the different entropic terms and the resulting $S_{\rm conf}$ for three different densities. Panel (d) also shows the PEL representation of $S_{\rm conf}$ according to Eq. (13), with

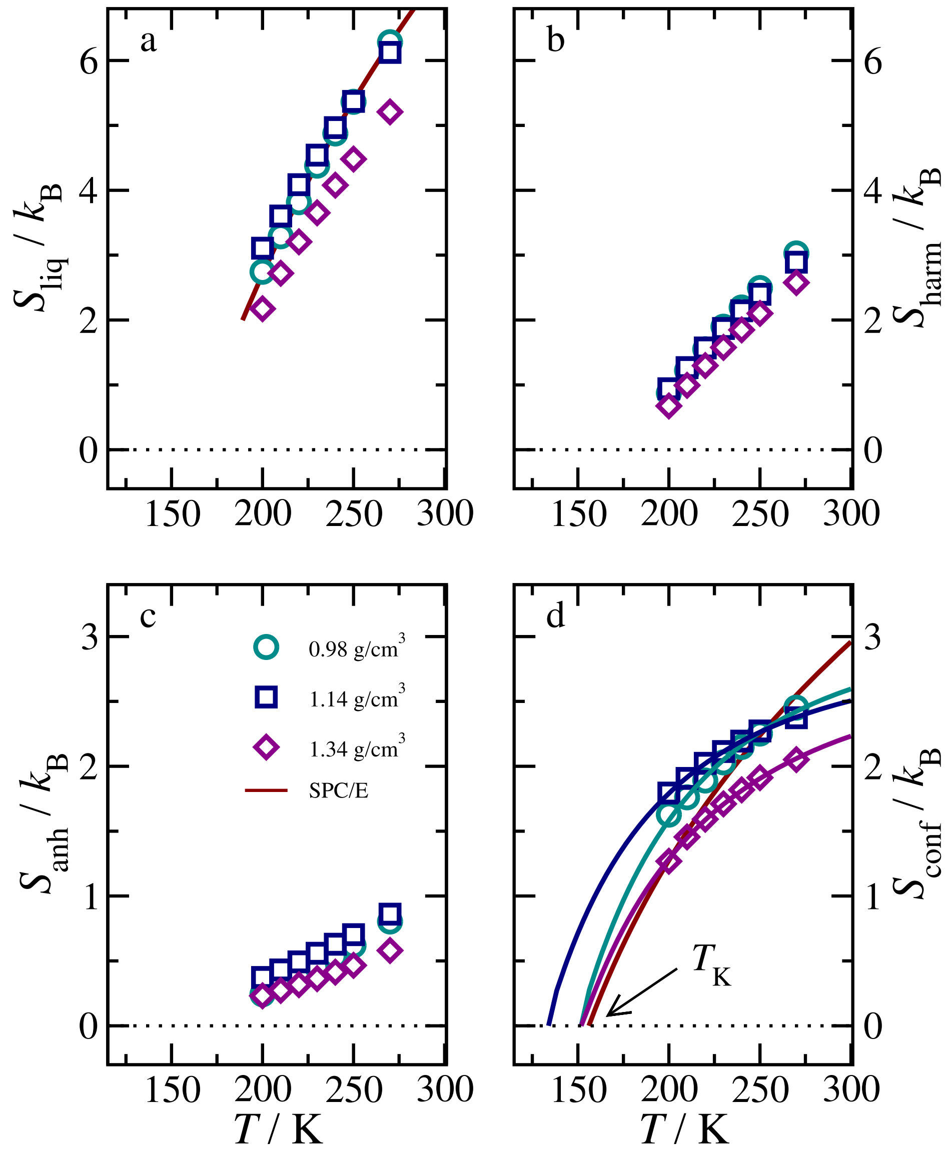

FIG. 9. Temperature dependence of the entropy of the liquid $S_{\rm liq}$ (a), of the vibrational entropy (both harmonic $S_{\rm harm}$ (b) and anharmonic $S_{\rm anh}$ (c) components), and of the resulting configurational entropy $S_{\rm conf}$ (d) for ρ = 0.98, 1.14, and 1.34 g/cm^3 in comparison with the result for SPC/E at ρ = 1.0 g/cm^3 from Ref. 68. The lines in (d) represent the corresponding fits for $S_{\rm conf}$ according to Eq. (13). All quantities are expressed as per particle.

α as the only fit parameter. The PEL theoretical expression properly models the T dependence of the numerical data. The extrapolation of the theoretical curves toward $S_{\text{conf}} = 0$ provides a visual estimate of the Kauzmann T. The resulting density dependence will be discussed in Sec. V C together with the landscape phase diagram. The ρ dependence of the best-fit values for α is shown in Fig. 7(c). α shows a monotonic dependence on ρ. The total number of basins, $\exp(\alpha N)$, increases on decreasing density, with a trend consistent with what has been observed in all other studied models.[29,46,50]

C. The PEL-EOS

The V derivatives of the landscape parameters allow us to evaluate the PEL-EOS [see Eq. (24)]. Figure 10 shows the polynomial fits for σ^2 [requested to evaluate $\mathcal{P}_{T^{-1}}$, Eq. (25)], for $E_0 - b\sigma^2$ [to evaluate $\mathcal{P}_{T^0}$, Eq. (26)], and for $\alpha - a + bE_0 + b^2\sigma^2/2$ [to evaluate $\mathcal{P}_{T^1}$, Eq. (27)]. The figure also shows the anharmonic contribution c_2 and c_3. The functional form has been chosen as a four-degree polynomial in V for σ^2, $E_0 - b\sigma^2$ and $\alpha - a + bE_0 + b^2\sigma^2/2$. Due to the larger numerical error in the anharmonic contribution, we select a quadratic function in V for c_2 and c_3. The resulting parameters are reported in Appendix B for future reference. The selection of a fourth order in the functional form generates a cubic V dependence of the pressure, which is the lowest order functional form consistent with the possibility of a liquid-liquid critical point.

The resulting set of fitting coefficients thus allow us to rebuild the PEL-EOS for all T. The corresponding PEL-EOS for selected isotherms is shown in Fig. 11 and compared with the MD results at the same T. We also compare our MD data as well as the PEL-EOS with the previously published isotherms from Biddle *et al.*[40] in Fig. 11. The PEL-EOS approximates the MD results rather well in the entire density range, stressing the ability of a Gaussian landscape thermodynamic approach to model the low T behavior of TIP4P/2005. As expected from the quality of the comparison, but also from the V-dependence of σ^2, the PEL-EOS predicts the existence of a temperature of maximum density (T_{MD}). The locus of the T_{MD} in the $P-T$ plane and in the $T-V$ plane is shown in Fig. 12, together with the MD results reported in the work of González *et al.*[69] In the same figure, we also show the projection of the Kauzmann locus, evaluated according to Eq. (14). Within the PEL paradigm, this locus signals the limit of validity of the PEL-EOS previously derived. For lower T, the configurational entropy vanishes, the system has reached the

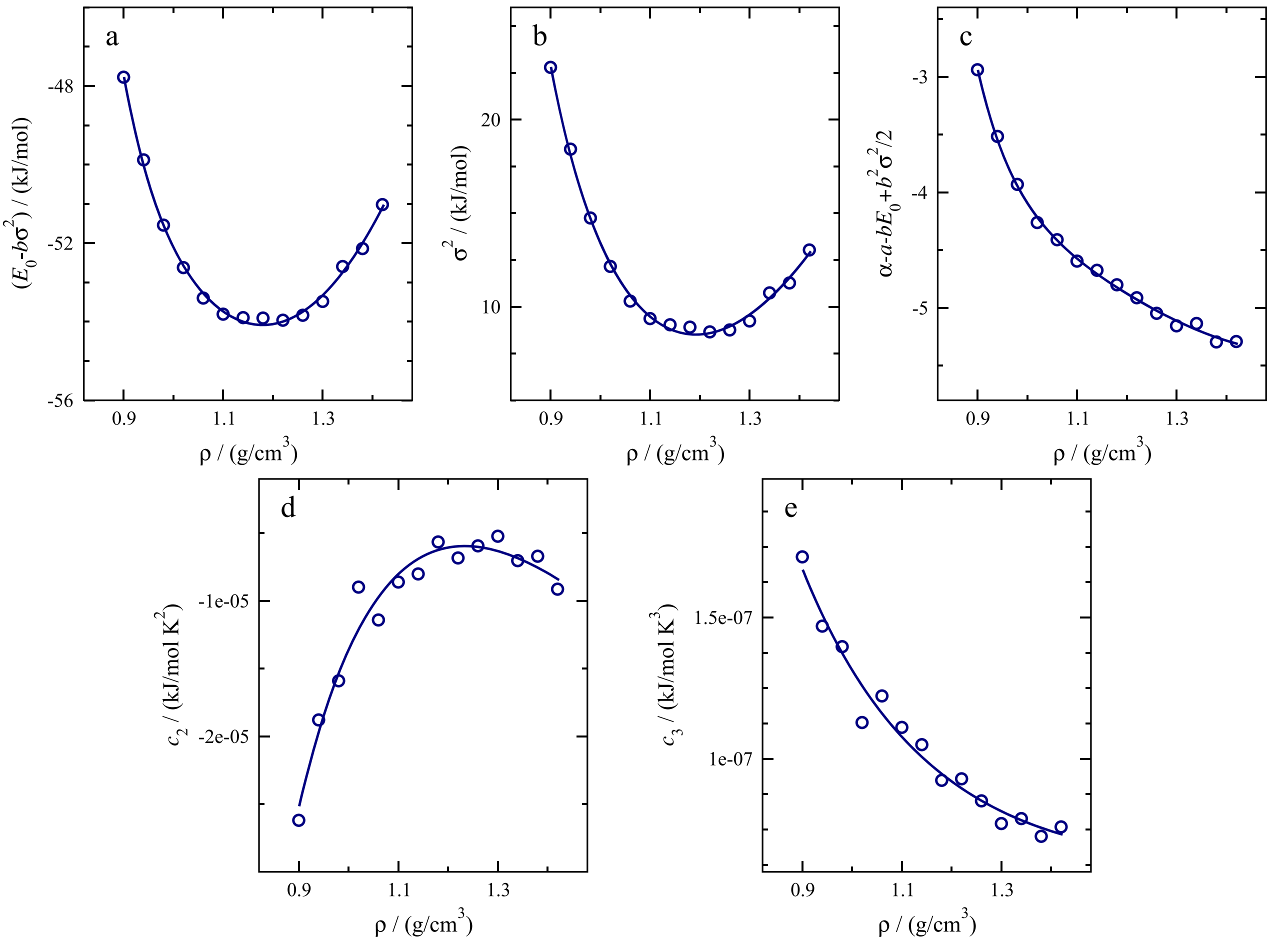

FIG. 10. Best polynomial fits in V of the quantities relevant for evaluating the PEL-EOS. The polynomial fit has degree four for the quantities in panels (a)–(c) [$E_0 - b\sigma^2$, σ^2 and $\alpha N - a - bE_0 + b^2\sigma^2/2$, cf. Eqs. (25)–(27)] and degree two for the quantities in panels (d) and (e) [c_2 and c_3, cf. Eq. (28)].

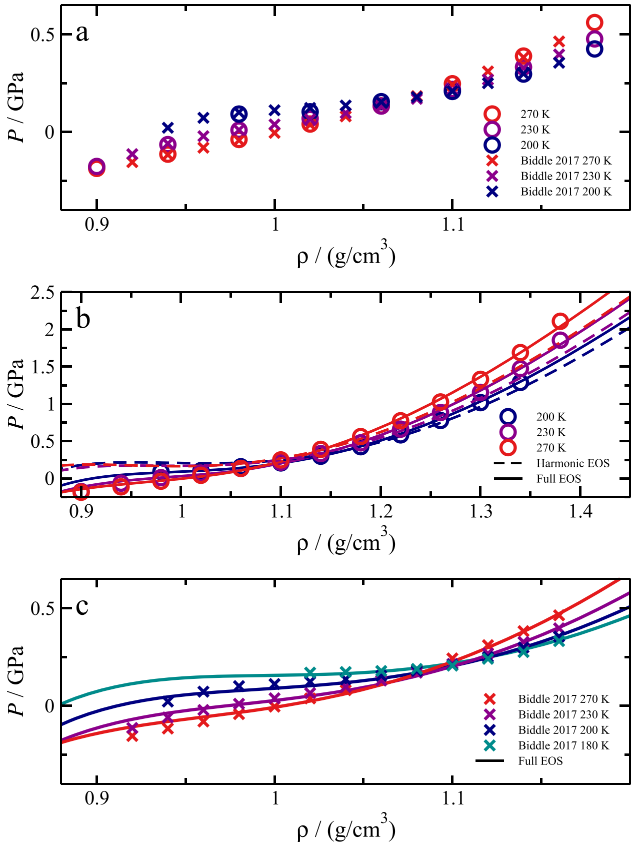

FIG. 11. Pressure-density isotherms. Panel (a) compares MD results from this study with recently published data from the work of Biddle *et al.*[40] Panel (b) compares the EOS resulting from the MD simulations with both the harmonic (dashed) and full (harmonic plus anharmonic, solid) landscape EOS. Panel (c) compares the EOS resulting from the MD simulations of Biddle *et al.*[40] with the full PEL-EOS including the extrapolation of the theoretical PEL prediction to $T = 180$ K, a T which was not studied in the present work.

ideal-glass state [the basin with energy e_K, see Eq. (15)], and the only residual contribution to the free-energy arises from the vibrational component. Please note that this extrapolation is only valid if the landscape remains Gaussian down to the evaluated T_K.

The derived PEL-EOS formally depends on the assumption of a Gaussian PEL. In this respect, it offers a sound formulation of the thermodynamics of the TIP4P/2005 model which can be extended to temperatures below the lowest investigated one with the only assumption that the landscape retains its Gaussian character. It has been observed[29] that a Gaussian PEL and a minimum in σ^2 vs. V are the only ingredients requested to generate a low T liquid-liquid critical point. Consistent with this prediction, we determine for the TIP4P/2005 model the T and P values of the liquid-liquid critical point from the simultaneous vanishing of the first and second V derivatives of the EOS. The best estimate is $T_c = 175$ K, $p_c = 0.175$ GPa, and $\rho_c = 0.9970$ g/cm^3. The location of the predicted critical point is also shown in Fig. 12. We note that small variations of the ρ-range included in the fit of the volume dependence of the landscape parameter do not significantly change the predicted critical parameters. We then conclude that the critical parameters, according to this approach, are accurate within $T_c \pm 2$ K, $p_c \pm 0.002$ GPa, and $\rho_c \pm 0.001$ g/cm^3. The PEL estimate has to be compared with the value of $T_c = 193$ K reported in Ref. 33 as well as with the more recent estimate $T_c = 182$ K.[35,39,40]

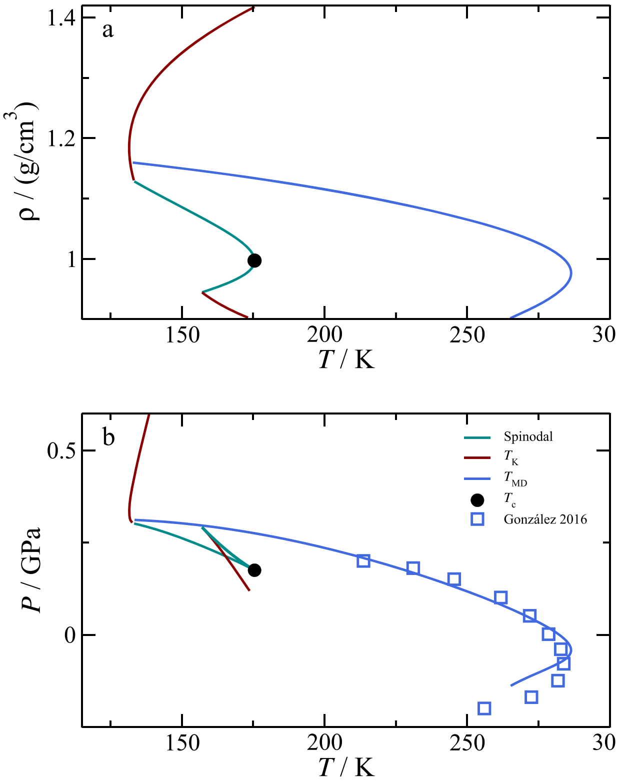

FIG. 12. Density-temperature (a) and pressure-temperature (b) PEL phase diagrams, reporting the liquid-liquid critical point and its associated mean-field spinodals, the Kauzmann T_K, and the T_{MD} loci. It also shows in (b) the MD results for the T_{MD} locus from Ref. 69.

VI. CONCLUSIONS

In this article, we have reported a thorough analysis of the potential energy landscape statistical properties for the TIP4P/2005 model, one of the most accurate classical models for water.[31] To do so, we evaluate the inherent structure and the local curvature around the IS for fourteen different densities and seven different temperatures.

We have shown that a Gaussian distribution of basin depth provides an accurate description of the system thermodynamics. In the Gaussian landscape, just three quantities (E_0, σ^2, and α) control the thermodynamic behavior of the system. We have found that each molecule contributes to approximately e^3 basins, a number very close to the one which had been calculated for SPC/E previously. From the volume derivative of these parameters, a landscape EOS has been derived. Interestingly, in harmonic approximation, the T-dependence of the P is condensed in three contributions, proportional to T^{-1}, T^0, and T^1, respectively. This simple T dependence makes it possible to identify immediately the PEL source of the density anomalies and the close connection between density anomalies and the existence of a liquid-liquid critical point. Indeed, we have confirmed that for TIP4P/2005 the variance of the Gaussian distribution is found to display a minimum as a function of the volume, the PEL signature of densities anomalies.

We have also shown that including the anharmonic contributions makes it possible to accurately describe the PEL free-energy and the corresponding EOS. The resulting PEL-EOS rather well approximates the MD $P(V, T)$, offering a reliable functional form for predicting the low T behavior of the model. A small T extrapolation predicts a liquid-liquid critical point in TIP4P/2005, consistent with previous estimates.[35,39,40]

Finally we note that in the present investigation we have not revealed any signature of failure of the Gaussian approximation. This is rather well documented in Fig. 6 where a deviation from a linear $1/T$ dependence is never observed. Still it is possible that, especially at low densities, where the system evolves toward a defect free tetrahedral network and the bottom of the landscape (the fully bonded network) is approached, the Gaussian approximation should reveal its large-number origin and cease pace to a logarithmic landscape.[11] A limited landscape analysis of the ST2 water model,[70,71] of silica,[62,72] and of tetrahedral patchy particles[73,74] suggests this as a concrete possibility, at least at the optimal network density. For the ST2 model, the landscape investigation at $\rho = 0.83$ g/cm^3 shows that, at low temperature, E_{IS} approaches a limiting value which has been identified as the energy of the fully bonded disordered tetrahedral network.[70] Not much is known instead of the ST2 PEL at densities around 1.0 g/cm^3, the ones relevant for developing an equation of state in the region where the liquid-liquid critical point is located. In light of the renewed interest in the ST2 potential (see, for example, Refs. 75 and 76), it might be worth considering performing a full landscape analysis of the ST2 model in the near future. The possibility to equilibrate configurations down to the liquid-liquid critical point for the ST2 model can provide a further stringent test of the ability to develop a full thermodynamic description via a PEL approach.

ACKNOWLEDGMENTS

P.H.H. thanks the Austrian Science Fund FWF for support (Erwin Schrödinger Fellowship No. J3811 N34). We also thank Chantal Valeriani for help in the initial stage of the project.

APPENDIX A: FREE ENERGIES OF SUPERCOOLED TIP4P/2005

In this section, we report the molar free energies F_{liq} of the TIP4P/2005 liquid at all studied state points in the T range 270-200 K. The values shown in Table I were evaluated from the thermodynamic integration technique explained in Sec. IV C.

APPENDIX B: PEL-EOS PARAMETERS

As explained in Sec. V C, we fitted the volume dependence of the quantities relevant for the PEL-EOS [cf. Eqs. (24)–(28)] by polynomials in molar volume V,

$$f(V) = \sum_{0}^{n} A_i V^i, \tag{B1}$$

where n was four for the arguments in Eqs. (25)–(27) and two for the V dependence of c_2 and c_3 [cf. Eq. (28)]. The resulting parameters, which suffice to build the PEL-EOS, are summarised in Table II.

TABLE I. Molar free energies F_{liq} in kJ mol^{-1} of the TIP4P/2005 liquid at given T and ρ.

	ρ (g/cm^3)													
T (K)	0.9	0.94	0.98	1.02	1.06	1.1	1.14	1.18	1.22	1.26	1.3	1.34	1.38	1.42
270	−56.91	−57.04	−57.10	−57.10	−57.04	−56.93	−56.74	−56.49	−56.16	−55.74	−55.23	−54.60	−53.87	−53.00
250	−55.96	−56.08	−56.13	−56.12	−56.06	−55.95	−55.79	−55.55	−55.25	−54.86	−54.38	−53.80	−53.11	−52.29
240	−55.56	−55.67	−55.70	−55.69	−55.63	−55.52	−55.36	−55.13	−54.84	−54.47	−54.00	−53.44	−52.77	−51.98
230	−55.20	−55.30	−55.32	−55.29	−55.23	−55.12	−54.96	−54.75	−54.46	−54.10	−53.66	−53.12	−52.47	. . .
220	−54.89	−54.98	−54.98	−54.94	−54.86	−54.76	−54.60	−54.40	−54.13	−53.78	−53.35	−52.84	−52.22	. . .
210	. . .	−54.70	−54.68	−54.62	−54.54	−54.43	−54.28	−54.08	−53.83	−53.50	−53.09	−52.59	. . .	. . .
200	. . .	. . .	−54.41	−54.35	−54.26	−54.15	−54.01	−53.81	−53.56	−53.25	−52.86	−52.38	. . .	. . .

TABLE II. Fitting parameters of the polynomial fit in V of the quantities (Q) relevant for the PEL-EOS. The unit of A_i is the unit of Q (cf. Fig. 10) times the unit of inverse molar volume (mol/cm^3) to the ith power.

Q	A_0	A_1	A_2	A_3	A_4
$E_0 - b\sigma^2$	$4.69736 \cdot 10^{2}$	$-1.19385 \cdot 10^{2}$	$1.02918 \cdot 10^{1}$	$-4.00425 \cdot 10^{-1}$	$5.98043 \cdot 10^{-3}$
σ^2	$5.50606 \cdot 10^{2}$	$-1.16995 \cdot 10^{2}$	$9.61032 \cdot 10^{0}$	$-3.63301 \cdot 10^{-1}$	$5.46496 \cdot 10^{-3}$
$\alpha N - a - bE_0 + b^2\sigma^2/2$	$5.08848 \cdot 10^{1}$	$-1.53888 \cdot 10^{1}$	$1.55381 \cdot 10^{0}$	$-6.90207 \cdot 10^{-2}$	$1.15370 \cdot 10^{-3}$
c_2	$-1.46726 \cdot 10^{-4}$	$1.92760 \cdot 10^{-5}$	$-6.59881 \cdot 10^{-7}$	. . .	. . .
c_3	$1.53829 \cdot 10^{-7}$	$-1.84834 \cdot 10^{-8}$	$9.56831 \cdot 10^{-10}$	. . .	. . .

[1] F. H. Stillinger, *Energy Landscapes, Inherent Structures, and Condensed-Matter Phenomena* (Princeton University Press, 2015).
[2] F. H. Stillinger and T. A. Weber, Phys. Rev. A **25**, 978 (1982).
[3] M. Goldstein, J. Chem. Phys. **51**, 3728 (1969).
[4] E. La Nave, S. Sastry, and F. Sciortino, Phys. Rev. E **74**, 050501 (2006).
[5] A. Heuer, J. Phys.: Condens. Matter **20**, 373101 (2008).
[6] S. Sastry, P. G. Debenedetti, and F. H. Stillinger, Nature **393**, 554 (1998).
[7] F. Sciortino, W. Kob, and P. Tartaglia, Phys. Rev. Lett. **83**, 3214 (1999).
[8] E. La Nave, S. Mossa, and F. Sciortino, Phys. Rev. Lett. **88**, 225701 (2002).
[9] A. Heuer and S. Büchner, J. Phys.: Condens. Matter **12**, 6535 (2000).
[10] P. G. Debenedetti, T. M. Truskett, C. P. Lewis, and F. H. Stillinger, Adv. Chem. Eng. **28**, 21 (2001).
[11] P. G. Debenedetti, F. H. Stillinger, and M. S. Shell, J. Phys. Chem. B **107**, 14434 (2003).
[12] M. S. Shell and P. G. Debenedetti, Phys. Rev. E **69**, 051102 (2004).
[13] F. Sciortino and P. Tartaglia, Phys. Rev. Lett. **86**, 107 (2001).
[14] P. G. Debenedetti, J. Phys.: Condens. Matter **15**, R1669 (2003).
[15] T. Loerting, K. Winkel, M. Seidl, M. Bauer, C. Mitterdorfer, P. H. Handle, C. G. Salzmann, E. Mayer, J. L. Finney, and D. T. Bowron, Phys. Chem. Chem. Phys. **13**, 8783 (2011).
[16] P. Gallo, K. Amann-Winkel, C. A. Angell, M. A. Anisimov, F. Caupin, C. Chakravarty, E. Lascaris, T. Loerting, A. Z. Panagiotopoulos, J. Russo *et al.*, Chem. Rev. **116**, 7463 (2016).
[17] P. H. Handle, T. Loerting, and F. Sciortino, Proc. Natl. Acad. Sci. U. S. A. **114**, 13336–13344 (2017).
[18] K. H. Kim, A. Späh, H. Pathak, F. Perakis, D. Mariedahl, K. Amann-Winkel, J. A. Sellberg, J. H. Lee, S. Kim, J. Park *et al.*, Science **358**, 1589 (2017).
[19] V. Holten, C. Qiu, E. Guillerm, M. Wilke, J. Ricka, M. Frenz, and F. Caupin, J. Phys. Chem. Lett. **8**, 5519 (2017).
[20] A. Nilsson and L. G. Pettersson, Nat. Commun. **6**, 8998 (2015).
[21] R. J. Speedy, J. Phys. Chem. **86**, 982 (1982).
[22] L. Rovigatti, V. Bianco, J. M. Tavares, and F. Sciortino, J. Chem. Phys. **146**, 041103 (2017).
[23] Y. Kalyuzhnyi and P. Cummings, J. Chem. Phys. **139**, 104905 (2013).
[24] S. Sastry, P. G. Debenedetti, F. Sciortino, and H. E. Stanley, Phys. Rev. E **53**, 6144 (1996).
[25] P. H. Poole, F. Sciortino, U. Essmann, and H. Stanley, Nature **360**, 324 (1992).
[26] M. A. Anisimov, M. Duška, F. Caupin, L. E. Amrhein, A. Rosenbaum, and R. J. Sadus, Phys. Rev. X **8**, 011004 (2018).
[27] L. P. N. Rebelo, P. G. Debenedetti, and S. Sastry, J. Chem. Phys. **109**, 626 (1998).
[28] P. H. Poole, I. Saika-Voivod, and F. Sciortino, J. Phys.: Condens. Matter **17**, L431 (2005).
[29] F. Sciortino, E. La Nave, and P. Tartaglia, Phys. Rev. Lett. **91**, 155701 (2003).
[30] H. J. C. Berendsen, J. R. Grigera, and T. P. Straatsma, J. Phys. Chem. **91**, 6269 (1987).
[31] C. Vega and J. L. Abascal, Phys. Chem. Chem. Phys. **13**, 19663 (2011).
[32] J. L. Abascal and C. Vega, J. Chem. Phys. **123**, 234505 (2005).
[33] J. L. Abascal and C. Vega, J. Chem. Phys. **133**, 234502 (2010).
[34] K. Wikfeldt, A. Nilsson, and L. G. Pettersson, Phys. Chem. Chem. Phys. **13**, 19918 (2011).
[35] T. Sumi and H. Sekino, RSC Adv. **3**, 12743 (2013).
[36] T. Yagasaki, M. Matsumoto, and H. Tanaka, Phys. Rev. E **89**, 020301 (2014).
[37] S. Overduin and G. Patey, J. Chem. Phys. **138**, 184502 (2013).
[38] S. Overduin and G. Patey, J. Chem. Phys. **143**, 094504 (2015).
[39] R. S. Singh, J. W. Biddle, P. G. Debenedetti, and M. A. Anisimov, J. Chem. Phys. **144**, 144504 (2016).
[40] J. W. Biddle, R. S. Singh, E. M. Sparano, F. Ricci, M. A. González, C. Valeriani, J. L. Abascal, P. G. Debenedetti, M. A. Anisimov, and F. Caupin, J. Chem. Phys. **146**, 034502 (2017).
[41] E. Burton and W. F. Oliver, Nature **135**, 505 (1935).
[42] P. Brüggeller and E. Mayer, Nature **288**, 569 (1980).
[43] O. Mishima, L. D. Calvert, and E. Whalley, Nature **310**, 393 (1984).
[44] T. Loerting, C. Salzmann, I. Kohl, E. Mayer, and A. Hallbrucker, Phys. Chem. Chem. Phys. **3**, 5355 (2001).
[45] P. H. Handle and T. Loerting, Phys. Chem. Chem. Phys. **17**, 5403 (2015).
[46] F. Sciortino, J. Stat. Mech.: Theory Exp. **2005**, P05015.
[47] F. H. Stillinger and P. G. Debenedetti, J. Chem. Phys. **116**, 3353 (2002).
[48] R. J. Speedy, J. Phys.: Condens. Matter **15**, S1243 (2003).
[49] N. Giovambattista, H. E. Stanley, and F. Sciortino, Phys. Rev. Lett. **91**, 115504 (2003).
[50] S. Mossa, E. La Nave, H. Stanley, C. Donati, F. Sciortino, and P. Tartaglia, Phys. Rev. E **65**, 041205 (2002).
[51] E. La Nave, F. Sciortino, P. Tartaglia, C. De Michele, and S. Mossa, J. Phys.: Condens. Matter **15**, S1085 (2003).
[52] M. S. Shell, P. G. Debenedetti, E. La Nave, and F. Sciortino, J. Chem. Phys. **118**, 8821 (2003).
[53] D. Van Der Spoel, E. Lindahl, B. Hess, G. Groenhof, A. E. Mark, and H. J. Berendsen, J. Comput. Chem. **26**, 1701 (2005).
[54] S. Nosé, Mol. Phys. **52**, 255 (1984).
[55] W. G. Hoover, Phys. Rev. A **31**, 1695 (1985).
[56] U. Essmann, L. Perera, M. L. Berkowitz, T. Darden, H. Lee, and L. G. Pedersen, J. Chem. Phys. **103**, 8577 (1995).
[57] B. Hess, J. Chem. Theory Comput. **4**, 116 (2008).
[58] E. La Nave and F. Sciortino, J. Phys. Chem. B **108**, 19663 (2004).
[59] C. Vega, E. Sanz, J. Abascal, and E. Noya, J. Phys.: Condens. Matter **20**, 153101 (2008).
[60] J. E. Mayer and M. G. Mayer, *Statistical Mechanics* (John Wiley & Sons, 1963).
[61] F. Smallenburg, P. H. Poole, and F. Sciortino, Mol. Phys. **113**, 2791 (2015).
[62] I. Saika-Voivod, P. H. Poole, and F. Sciortino, Nature **412**, 514 (2001).
[63] F. Sciortino, P. H. Poole, U. Essmann, and H. Stanley, Phys. Rev. E **55**, 727 (1997).
[64] N. Giovambattista, F. W. Starr, and P. H. Poole, J. Chem. Phys. **147**, 044501 (2017).
[65] S. Torquato and F. H. Stillinger, Phys. Rev. E **68**, 041113 (2003).
[66] F. Martelli, S. Torquato, N. Giovambattista, and R. Car, Phys. Rev. Lett. **119**, 136002 (2017).
[67] P. Kumar, K. T. Wikfeldt, D. Schlesinger, L. G. Pettersson, and H. E. Stanley, Sci. Rep. **3**, 1980 (2013).
[68] A. Scala, F. W. Starr, E. La Nave, F. Sciortino, and H. E. Stanley, Nature **406**, 166 (2000).
[69] M. A. González, C. Valeriani, F. Caupin, and J. L. Abascal, J. Chem. Phys. **145**, 054505 (2016).
[70] P. H. Poole, S. R. Becker, F. Sciortino, and F. W. Starr, J. Phys. Chem. B **115**, 14176 (2011).
[71] N. Giovambattista, F. Sciortino, F. W. Starr, and P. H. Poole, J. Chem. Phys. **145**, 224501 (2016).
[72] A. Saksaengwijit, J. Reinisch, and A. Heuer, Phys. Rev. Lett. **93**, 235701 (2004).
[73] A. Moreno, I. Saika-Voivod, E. Zaccarelli, E. La Nave, S. Buldyrev, P. Tartaglia, and F. Sciortino, J. Chem. Phys. **124**, 204509 (2006).
[74] F. Smallenburg and F. Sciortino, Nat. Phys. **9**, 554 (2013).
[75] J. C. Palmer, F. Martelli, Y. Liu, R. Car, A. Z. Panagiotopoulos, and P. G. Debenedetti, Nature **510**, 385 (2014).
[76] F. Smallenburg and F. Sciortino, Phys. Rev. Lett. **115**, 015701 (2015).